Available online at www.sciencedirect.com
SCIENCE DIRECT®
Journal of Catalysis 221 (2004) 500–509
JOURNAL OF CATALYSIS
www.elsevier.com/locate/jcat

Effect of confinement on the selectivity of hydrocracking

H. Toulhoat,[a,*] P. Raybaud,[b] and Eric Benazzi [c]

[a] *Direction Scientifique, Institut Français du Pétrole, 1 & 4 avenue de Bois-Preau, 92852 Rueil-Malmaison cedex, France*
[b] *Division Chimie et Physico-Chimie Appliquées, Institut Français du Pétrole, 1 & 4 avenue de Bois-Preau, 92852 Rueil-Malmaison cedex, France*
[c] *Division Cinétique et Catalyse, Institut Français du Pétrole, 1 & 4 avenue de Bois-Preau, 92852 Rueil-Malmaison cedex, France*

Received 18 June 2003; revised 14 August 2003; accepted 10 September 2003

Abstract

We present molecular simulation results for the adsorption of a set of hydrocarbons in model zeolite structures of various pore sizes. Average adsorption energies scale approximately linearly with the cubic root of the ratio of molecular volume to maximal molecular volume. The maximal molecular volume depends on the zeolite structure and characterizes a steric exclusion threshold. This behavior is consistent with the confinement theory introduced by Derouane and co-workers. We use this result in a simplified model of the effect of confinement in hydrocracking, in order to better understand the respective roles of acidity and confinement on the selectivity toward products of intermediate molecular weight. We show that selectivity is determined by the profile of activity as a function of pore size and/or maximal molecular volume, itself mostly determined by the confinement effect. These findings have important practical implications for the design of hydrocracking catalysts with a prescribed selectivity.

Keywords: Mathematical model of hydrocracking; Bifunctional catalyst; Zeolites; Silica–alumina; Confinement; Adsorption; Molecular simulation

1. Introduction

In a recent paper [1], it has been shown experimentally that the key factor determining the distribution of hydrocracked products is the pore size of the bifunctional catalyst selected to convert a particular feedstock: indeed, under conditions of ideal hydrocracking, namely when the hydrogenating-dehydrogenating function is not limiting, at a given temperature and a given total conversion, the yield in the most valuable products of intermediate molecular weight, or selectivity, increases with the pore size. Moreover, while the activity increases in proportion to the strength and density of acid sites, the selectivity is hardly affected by the acidity. The interpretation already presented in [1] points out the significance of the adsorption strength of primary cracking products within the catalyst's pores, as overcracking can result from a too strong adsorption. As shown by Derouane and co-workers [2–4], the adsorption strength is strongly dependent on the molecule to pore size ratio via the so-called "confinement effect." We expect, therefore, that the problem of selecting the optimal pore size for a hydrocracking catalyst has no unique solution: each solution will actually depend on the feedstock's average molecular weight and structure, and on the desired slate of products. The goal of the present communication is to help rational optimization on the basis of a simple mathematical model and molecular simulations of confinement effects.

2. Methods

2.1. Molecular simulation

We have used the grand canonical Monte Carlo technique, as implemented in the Sorption module of Cerius^2 release 4.0 [5], in order to evaluate adsorption loadings and enthalpies at equilibrium inside model microporous networks, at a given temperature ($T = 573$ K) and pressure ($P = 100$ kPa), consistent with the conditions of catalytic experiments reported in [1]. Adsorption was simulated for hydrocarbons corresponding to intermediates and products in the hydrocracking of phenanthrene as observed in [1], in ideal siliceous frameworks for various relevant zeolitic structures. Some linear alkanes were added to this set of molecules. At high temperatures, hydrocarbon molecules are

* Corresponding author.
E-mail address: herve.toulhoat@ifp.fr (H. Toulhoat).

0021-9517/$ – see front matter
doi:10.1016/j.jcat.2003.09.014

distributed over several sites within the zeolite framework; the "location" becomes a probability distribution and the energy an integral over all accessible sites. In the grand canonical ensemble (μVT), the Metropolis algorithm proceeds by selecting, displacing, inserting, and deleting randomly a molecule. The Metropolis scheme generates a Markov chain of states which sample the equilibrium states of the system according to the Boltzmann probability distribution. Equilibrium is achieved when T and μ of the compounds inside the zeolite are equal to those of the free molecule in the gas phase. Depending on the system and on the hydrocarbon, the number of search iterations varies between 10^6 and 5×10^6 before reaching the convergence criterion on the energy (0.1 kJ mol^{-1}). The atoms of the zeolite framework are kept fixed and the hydrocarbons are supposed rigid; therefore, only the nonbonded terms in the force field are involved in the energy calculation at each Monte Carlo step. We have used the Universal Force Field (UFF release 1.02) as implemented in Cerius^2 according to Rappe et al. [6]. The zeolitic frameworks were represented by repeated unit cells with three-dimensional periodic boundary conditions. The van der Waals interactions were considered only in a sphere within a finite radius, called the cutoff radius, and using the long-range tail correction [7]. We have verified the convergence of the energy with respect to the cutoff.

2.2. A simplified mathematical model for hydrocracking

From the refiner's point of view, a primary characteristic of a hydrocarbon feedstock is its distillation curve, or equivalently the distribution function of its components according to molecular weight. Hydrocracking is essentially a process designed to modify in a controlled way this distribution function, so as to achieve the slate of product fuels corresponding to market demand. In what follows, we propose a simplified mathematical model of hydrocracking in confining pore space, which takes into account the influences of molecular weight M, and microporous structure on reactivity. The feedstock is characterized by an initial distribution function DF°(M), and the model provides as output the distribution function DF(M, θ) as a function of contact time θ.

The catalytic reactor is represented by a matrix of interconnected ideally mixed reactors $[R_{i,j}]$ offering the same reaction volume V_r, where a row of index i corresponds to the fraction $i\Delta\theta$ of the total contact time θ, and a column of index j corresponds to the molecular weight $M_j = j\Delta M + M_0$ (see scheme in Fig. 1). Each reactor $R_{i,j}$ contributes to cracking: it is fed by all reactors of the preceding row $R_{i-1,k}$ such that $k \geqslant j$, while it feeds all reactors of the next row $R_{i+1,k}$ such that $k \leqslant j$. Reactors $R_{0,j}$ are inactive storage tanks feeding the first active row $R_{1,j}$. Reactors of the last row $R_{N,j}$, where $N = \theta/\Delta\theta$, are inactive storage tanks gathering the final products. A mass fraction per unit of reaction volume $m_{i,j}$ is associated to each matrix element or partial reactor, and the first row $m_{0,j}$ represents

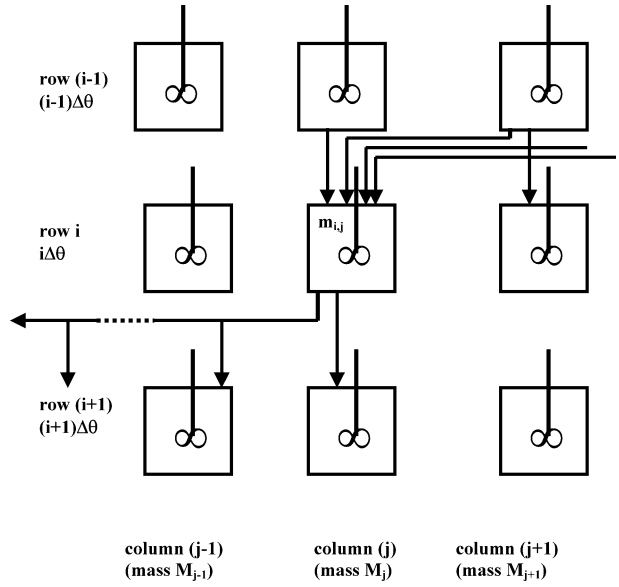

Fig. 1. Scheme of our hydrocracking model. Each virtual elementary stirred tank reactor $R_{k,j}$ selects mass M_j. It is fed by all the reactors in the preceding row, of equal or higher column number, and feeds all reactors of the next row of equal or lower column number. Arrows symbolize flows of mass to and from reactor $R_{i,j}$.

the distribution function in mass of the feedstock. The corresponding concentration is therefore $C_{i,j} = m_{i,j}/(M_j V_r)$. The sum $\sum_{j=1}^{j=N} m_{i,j}$ is conserved from row to row.

In the next step, we express $m_{i,j}$ as a function of inputs and ouput in each elementary reactor $R_{i,j}$: we retain the simplifying assumption that C–C bonds will crack randomly in saturated hydrocarbons, so that a molecule of mass M_k will fragment with equal probability into lighter molecules of every possible mass $M_{j<k}$. Using the integrated expression giving the concentration versus contact time for a first-order reaction in an ideally mixed reactor, we obtain for $m_{i,j}$ the following sum where the first term accounts for the unreacted amount after $\Delta\theta$ of molecules of mass M_j transferred from reactor $R_{i-1,j}$ to reactor $R_{i,j}$, and the second term collects all amounts of mass M_j produced by the random cracking of higher masses $M_{k>j}$ in reactors $R_{i-1,k}$ in the $\Delta\theta$ interval:

$$m_{i,j} = m_{i-1,j}\exp(-k_j\Delta\theta) + \sum_{j+1}^{N} m_{i-1,l}\frac{1-\exp(-k_l\Delta\theta)}{l-1}. \quad (1)$$

In Eq. (1) k_j is the rate constant of catalytic cracking, which depends on the molecular mass M_j, thus on the column index j, as demonstrated below.

Within the transition state theory (TST) and following Derouane [4] in the assumption of cracking being a first-order reaction with respect to the hydrocarbon reactant of mass M_j, the rate of cracking r_j can be written as

$$r_j = \frac{kT}{h}\exp\left(\frac{-\Delta G^{\pm}}{kT}\right)\sigma^* C_j^{\text{pore}} = k_j C_j, \quad (2)$$

where k and h are the Boltzmann and Planck constants, T the temperature, $\Delta G^{\pm}$ the free energy of activation of the cracking reaction, and σ^* the volumic density of acid sites, both assumed independent of the index j, but depending in principle on the porous solid which catalyzes the cracking reaction. C_j^{pore} is the concentration of species of molecular volume $V_{\text{m}j}$ or molecular mass M_j in the confined porous space, in equilibrium with the concentration C_j in free space.

Here, the adsorption isotherm C_j^{pore} (C_j) takes into account the so-called confinement effect. In reality, it is a multicomponent isotherm, quite difficult to determine in the present state of the art, either from experiments or from simulations. In what follows, we assume that concentrations in every component remain low enough at any contact time and for any molecular mass that individual adsorption isotherms remain in the Henry linear regime and that interactions between different species remain negligible. Therefore we write

$$C_j^{\text{pore}} \cong K_j^{\text{H}} C_j \cong \exp\left(\frac{-\Delta G_j^{\text{ads}}}{kT}\right) C_j, \tag{3}$$

where K_j^{H} is the Henry constant of component j, and $\Delta G_j^{\text{ads}} = \Delta H_j^{\text{ads}} - T\Delta S_j^{\text{ads}}$ is the free energy of adsorption of component j in the limit of vanishing C_j, for a particular porous solid. ΔH_j^{ads} is the heat of adsorption, and ΔS_j^{ads} the entropy of adsorption.

The "toy" model specified by Eqs. (1) to (3) can be conveniently implemented with a standard spreadsheet software (we have used MS Excel 97).

3. Results

The GCMC simulation results for adsorptions at 573 K and 100 kPa of molecules ranging from methane to tetrahydrophenanthrene are reported in Table 1, along with the corresponding molecular volumes V_{m}. The molecular volumes are molecular descriptors, estimated as the volumes of the solid envelope of overlapping van der Waals spheres centered on nuclei in the energy minimized structures at 0 K. The calculation of these descriptors is provided within the Cerius^2 software [5]. Table 1 shows equilibrium adsorptions, expressed in terms of concentrations in the pores, as well as the corresponding average adsorption energies. The adsorptions, in molecules per unit cell, resulting from the simulations, are expressed as concentrations in the pores, by taking into account the relevant void fractions, as presented in Table 2. For each microporous structure, the concentrations in the pores are plotted against V_{m} in Fig. 2. This figure reveals several phenomena: a first obvious trend is that equilibrium concentrations in pores systematically go through a very distinct maximum as V_{m} increases. Beyond this maximum, the equilibrium concentration decreases approximately linearly for the larger pores structures. In the case of MFI, there is no adsorption beyond a threshold of V_{m} equal to 0.170 nm^3. Naphthalene (0.127 nm^3) is excluded from MFI, while linear heptane (0.131 nm^3) adsorbs in the main channels. An intermediate behavior is found for offretite (OFF). These results allow us to define V_{mmax} as the molecular volume beyond which no adsorption occurs inside the microporous structure. V_{mmax} values reported in Table 2 correspond to the extrapolation to concentration zero of linear trends exhibited in Fig. 3 for the MFI, OFF, BETA, FAU, and VFI microporous structures. In the case of MFI, we have excluded aromatics (benzene and naphthalene) to obtain a linear trend, with the justification that, under ideal hydrocracking conditions, these molecules have already been hydrogenated into their fully saturated counterparts.

The case of MFI emphasizes clearly one limit of our approach which cannot differentiate molecules by their aspect ratio. A truly accurate prediction of steric exclusion should indeed include adequate descriptors of molecular shapes and pore geometries. Besides, as shown recently by Schenk et al. [9], molecular shape-dependent entropic effects are likely to play a role at high loading. The rough description we adopt here will hence apply mostly to reasonably bulky molecules, such as branched and hemicyclic hydrocarbons which are generally major components of hydrocracking feedstocks.

It is natural to confront the behavior discussed above to the predictions of the confinement model developed by Derouane et al. [2–4] for model geometries. When wall repulsions are taken into account as well as attractive dispersion forces, this model predicts that adsorption energy presents a distinct maximum as a function of the ratio $1/s = \sigma_{\text{e}}/R$ of the radii of curvature of the sorbate and pores, both being assumed spherical [3]. The parameter σ_{e} is the pair equilibrium distance in a two-body Lennard–Jones potential function modeling the physisorptive interaction. In the present case, we deal with very different shapes of molecules and pores and a common definition of s is not trivial. Since we can assume as a first approximation $V_{\text{m}} = \lambda\sigma_{\text{e}}^3$ and $V_{\text{mmax}} = \lambda\sigma_{\text{emax}}^3$, with $\sigma_{\text{emax}} = R/0.74$, the equilibrium distance above which the adsorption energy becomes positive according to [3], it is possible to use $s' = (V_{\text{m}}/V_{\text{mmax}})^{1/3} = 0.74/s$ as an equivalent to s. Indeed, as shown in Fig. 4, when $E_{\text{ads}} \sim \Delta H_j^{\text{ads}}$ is plotted against s', a master correlation of reasonable quality is obtained, which presents features similar to those predicted by Derouane (see Fig. 1 in [4]), namely an increasing part up to a maximum for $s'^* \sim 0.95$, here approximately linearly, followed by an abruptly decreasing branch between $s' = 0.95$ and 1. Moreover, when the adsorption enthalpy is appropriately rescaled, assuming $E_{\text{ads}} \sim \Delta H_j^{\text{ads}} \propto V_{\text{m}}$, a closer comparison with the numerical results provided by Derijcke et al. in [3] is possible, as shown in Fig. 5. The confinement effect manifests itself as an enhancement by a factor of about 2 of the rescaled adsorption energy between $s' \sim 0.45$ (methane in VFI) and s'^*, in relatively good agreement with the prediction by Derijcke et al., whereas the repulsion by pore walls induces the

Table 1
GCMC simulation results at 573 K and 100 kPa

	V_m (nm^3)	E_{ads}(MFI) (kcal mol^{-1})	C_{eq}(MFI) (mol L^{-1})	E_{ads}(OFF) (kcal mol^{-1})	C_{eq}(OFF) (mol L^{-1})
Methane	0.029	7.7	4.1	5.5[a]	2.4
Ethane	0.046	13.7	22.0	9.5[a]	13.0
Propane	0.063	19.7	23.6	14.55[a]	17.7
Butane	0.080	25.1	19.2	18.75[a]	16.9
Benzene	0.084	21.4	8.8	24.9	9.6
Methylcyclohexane	0.127	32.0	8.7	29.3	8.8
Naphthalene	0.127	24.6	0.7	29.1	3.9
Heptane	0.131	36.9	8.8	27.1	5.9
Phenanthrene	0.171	0.0	0.0	33.6	1.7
Methylcyclopentanodecalin	0.215	0.0	0.0	40.3	3.3
Perhydrophenanthrene	0.215	0.0	0.0	44.9	1.7
Dimethylcyclopentanomethylcyclohexane	0.227	0.0	0.0	46.0	3.9
Tetrahydrophenanthrene	0.227	0.0	0.0	35.3	0.7
	V_m (nm^3)	E_{ads}(Beta) (kcal mol^{-1})	C_{eq}(Beta) (mol L^{-1})	E_{ads}(FAU) (kcal mol^{-1})	C_{eq}(FAU) (mol L^{-1})
Methane	0.029	5.4	1.0	3.9[b]	1.5
Ethane	0.046	9.7	7.9	5.87[b]	3.6
Propane	0.063	14.7	13.9	10.12[b]	7.3
Butane	0.080	19.3	13.2	15.4	8.6
Benzene	0.084	22.9	15.4	20.2	11.3
Methylcyclohexane	0.127	29.8	10.1	25.3	7.7
Naphthalene	0.127	31.5	10	32	8.1
Heptane	0.131	29.1	9.6	25.5	6.8
Phenanthrene	0.171	36.7	5.9	39.4	5.7
Methylcyclopentanodecalin	0.215	48.0	5.0	40.2	4.4
Perhydrophenanthrene	0.215	46.4	4.4	38.6	4.2
Dimethylcyclopentanomethylcyclohexane	0.227	40.3	4.1	36.4	3.7
Tetrahydrophenanthrene	0.227	43.8	4.0	39.5	3.6
	V_m (nm^3)	E_{ads}(VFI) (kcal mol^{-1})	C_{eq}(VFI) (mol L^{-1})		
Methane	0.029	3.6	0.2		
Ethane	0.046	5.9	0.6		
Propane	0.063	8.6	2.3		
Butane	0.08	13.3	6.4		
Benzene	0.084	17.5	9.5		
Methylcyclohexane	0.127	23.6	7.3		
Naphthalene	0.127	28.6	7.3		
Heptane	0.131	23.7	6.2		
Phenanthrene	0.171	37.9	5.5		
Methylcyclopentanodecalin	0.215	36.5	3.9		
Perhydrophenanthrene	0.215	37.2	3.9		
Dimethylcyclopentanomethylcyclohexane	0.227	36.6	3.4		
Tetrahydrophenanthrene	0.227	35.1	3.3		

[a] Adsorption in 12 MR ring.
[b] Adsorption in supercage.

rapid decrease towards 0 beyond s'^*, as s' approaches 1. We assign most of the deviation of our simulation results with respect to the prediction of Derijcke et al. in Fig. 5 to the fact that actual molecules and actual pores are not spherical. The best agreement is found for FAU and VFI, the supercages of which have the closest shapes to spheres.

In the cases of FAU and OFF only, the simulations were performed without limiting the sampling to accessible volume, since the smaller alkanes also adsorb in the sodalite cages and 8MR channels, respectively. This leads to bimodal distributions of the adsorption energy. Since larger molecules are in reality excluded from the smaller cages or channels, we retain only the maximum of the peak at the higher energy (less negative) as corresponding to the average adsorption energy in the larger channels, in order to establish consistent correlations between adsorption energy and pore radii.

The implication of a rate law of order one with respect to sorbate concentration within the pores, as introduced under Methods, is that according to Fig. 2, the rate of cracking will depend strongly on V_m, or equivalently the molecular weight M, and on the type of microporous structure, for

Table 2
Characteristics of model microporous solids

	Vol. sim. box (nm^3)	Vol. occ. (nm^3)	Void fraction	V_{mmax} (nm^3)	Eq. CN	PD (nm)
MFI	42.65	5.94	0.14	0.17	11	0.55
OFF	18.56	3.32	0.18	0.24	15	0.67
BETA	16.93	3.89	0.23	0.28	18	0.7
FAU	15.68	5.27	0.34	0.30	19	0.74
VFI	40.43	13.32	0.33	0.31	20	1.27

Vol. sim. box, volume of the simulation supercell; Vol. occ., occupiable volume; void fraction, ratio Vol. occ./Vol. sim. box; V_{mmax}, maximal molecular volume beyond which no adsorption occurs inside the microporous structure; Eq. CN, equivalent carbon number calculated according to $j \cong V_{mmax}14/0.22$; PD, nominal pore diameter according to the IZA Atlas, 5th ed.

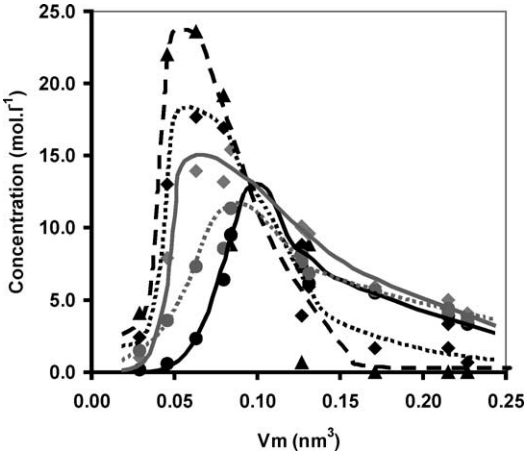

Fig. 2. Equilibrium concentrations of selected reaction products at 573 K and 100 kPa for model zeolites versus molecular volume (data from Table 1). Black triangles, MFI; black diamonds, OFF; gray diamonds, BETA; gray dots, FAU; black dots, VFI. Full lines are drawn for visual comfort.

given partial pressure of reactant in the free gas phase, temperature, and density and strength of acid sites, provided that the hydrogenating function is not limiting ("ideal hydrocracking").

By way of illustration, we choose to consider the hydrocracking of a feedstock comprising saturated even numbered C_n bulky hydrocarbons (that is, considerably branched, and/or naphthenic), with n ranging from 2 to 32. We assume that cracking will produce again even numbered C_n. The initial distribution m_{0j} is set according to a normal law, centered on $j = 18$, with a standard deviation of 2.

For the evaluation of the heats of adsorption, we use first the results presented in Fig. 4, modeled by a sawtooth function, the initial ramp of which can be expressed as

$$\Delta H_j^{\text{ads}} = -82.4\left(\frac{V_{\text{m}j}}{V_{\text{mmax}}}\right)^{1/3} + 36 \quad (\text{kcal mol}^{-1}), \qquad (4)$$

where V_{mmax} specifies the particular microporous solid considered. We moreover make use for alkanes of the correlation $V_{mj} = 0.01697j + 0.0186$ (nm^3). We avoid the use of Eq. (4) outside of the range of data for which the correlation was established, that is for $s' > 0.45$. This is the

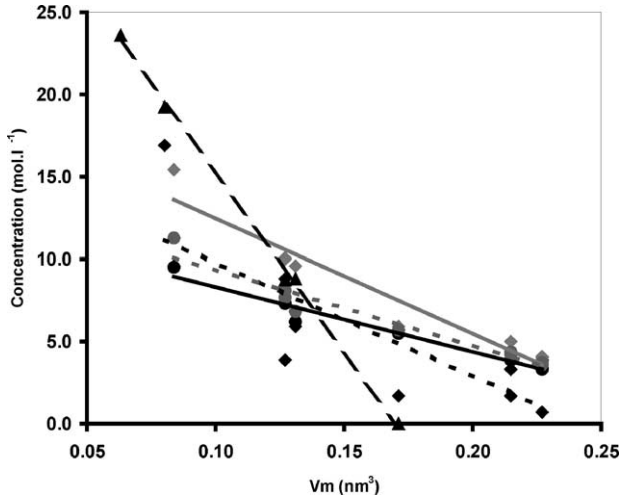

Fig. 3. Equilibrium concentrations of selected reaction products at 573 K and 100 kPa for model zeolites versus molecular volume beyond the maximum concentration (data from Table 1). Black triangles, MFI (benzene and naphthalene excluded); black diamonds, OFF; gray diamonds, BETA; gray dots, FAU; black dots, VFI. The straight lines are linear regressions allowing determination of V_{mmax} by extrapolation to concentration zero: MFI, $C_{eq} = -216.8V_m + 36.9$, $R^2 = 0.998$ (black broken line), $V_{mmax} = 0.17$ nm^3; OFF, $C_{eq} = -69.0V_m + 16.7$, $R^2 = 0.66$ (black dotted line), $V_{mmax} = 0.24$ nm^3; BETA, $C_{eq} = -70.2V_m + 19.5$, $R^2 = 0.94$ (gray line), $V_{mmax} = 0.28$ nm^3; FAU, $C_{eq} = -46.2V_m + 13.99$, $R^2 = 0.94$ (gray dotted line), $V_{mmax} = 0.30$ nm^3; VFI, $C_{eq} = -39.5V_m + 12.30$, $R^2 = 0.97$ (black line), $V_{mmax} = 0.31$ nm^3.

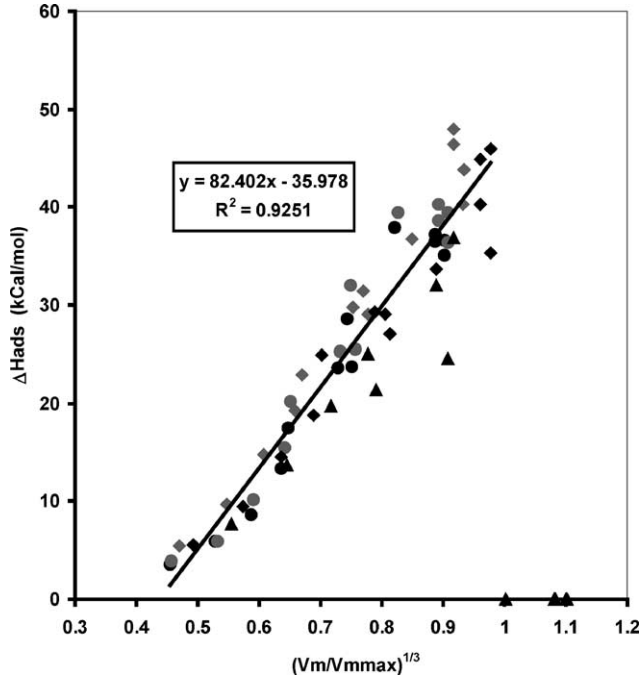

Fig. 4. Correlation between the heat of adsorption of selected products in model zeolites and the parameter s' as defined in the text. Black line, linear regression for data below $s' = 1$ and excluding aromatics in MFI. Black triangles, MFI; black diamonds, OFF; gray diamonds, BETA; gray dots, FAU; black dots, VFI (data from Table 1). Inset: regression line equation and coefficient of correlation.

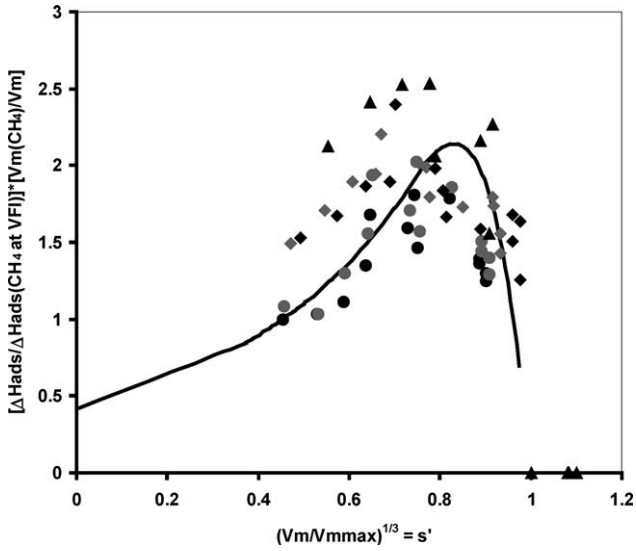

Fig. 5. Comparison of our simulation results with the prediction of the confinement theory. Black line, numerical estimate by Derijcke et al. [3] for spherical sorbates in spherical pores, assuming a 6–12 Lennard–Jones pair potential, rescaled with reference to methane adsorption in VFI. Black triangles, MFI; black diamonds, OFF; gray diamonds, BETA; gray dots, FAU; black dots, VFI (data from Table 1).

case for the reference silica–alumina, or alumina binder of zeolitic materials, which have average pore diameters of about 8 nm, to be compared to 1.27 nm for VFI. Indeed, the ratios of V_{mmax} for these two solids should be of the order of $(8/1.27)^3 \cong 250$, leading to $j[V_{\mathrm{mmax}}] \cong 5 \times 10^3$. Therefore, in the range $j = 2$ to 32 for instance, s' varies between 0.074 and 0.186. From the numerical estimate by Derijcke et al. for spheres in spheres, reported as a full line in Fig. 5, one expects the confinement effect to be very weak in this range. This effect can be represented by the linear approximation $f(s') = 0.257s' + 0.42$, so that one gets for the mesoporous amorphous supports in the range of s' below 0.19:

$$\Delta H_j^{\mathrm{ads}} = \Delta H_j^{\mathrm{ads}}[\mathrm{CH_4\ at\ VFI}](0.257s' + 0.42)\, j \quad (\mathrm{kcal\,mol^{-1}}) \quad \text{with } s'(j) \approx (j/5000)^{1/3}. \tag{5}$$

Our simulations resulted in estimates of $\Delta H_j^{\mathrm{ads}}$ at 573 K and $P_j = \mathrm{RTC}_j = 100$ kPa for the various microporous solids as listed in Table 1. In Eq. (3), according to the simplifying assumption retained, we need, however, the heat of adsorption of component j in the limit of vanishing C_j: we have verified that the differences between these enthalpies remain of the second order, so that numbers in Table 1 can be used reasonably in Eq. (3).

We then define the conversion of C_{14+} at contact time $i\,\Delta\theta$ as

$$(\mathrm{Conv\ C_{14+}})_i = 1 - \frac{\sum_{j=14}^{j=N} m_{ij}}{\sum_{j=1}^{j=N} m_{ij}} \tag{6}$$

Table 3
Experimental acidities and activities of zeolite-based hydrocracking catalysts (0.15% Pt in 5% zeolite + 95% alumina binder, or 0.15% Pt in silica(30%)–alumina(70%)

	Acidity (a.u.)	Activity (10^{-2} mol g^{-1} h^{-1})	Selectivity (%) at 60% conversion
MFI	8.30	4.60	(Conversion < 33%)
BETA	14.50	8.00	29
FAU 1	25.00	12.00	36
SiAl	2.00	0.02	48
FAU 2	9.70	5.30	36
FAU 3	2.00	1.20	41
FAU 4	0.60	0.60	46

Hydrocracking of perhydrophenanthrene (PHP) at 573 K and under 6 MPa (adapted from [1] and [8]). Selectivity means yield in C_{14} products at 60% conversion of PHP (reached at variable LHSV).

and the selectivity in "middle distillates" or fraction C_{10}–C_{14} as

$$(\mathrm{Sel\ C_{10}–C_{14}})_i = \frac{\sum_{j=10}^{j=14} m_{ij}}{\sum_{j=1}^{j=N} m_{ij}}. \tag{7}$$

We set $T = 573$ K and $\Delta H^{\pm} = 48$ kcal mol^{-1}. This value was chosen so as to match the apparent energy of activation $E_{\mathrm{app}}^{\pm}$ of 25 kcal mol^{-1} found experimentally for the ideal hydrocracking of phenanthrene on a Pt/SiO_2–Al_2O_3 catalyst [8]. According to Eqs. (2) and (3), we should have indeed $E_{\mathrm{app}}^{\pm}(\mathrm{C_{14}, SiAl}) = \Delta H^{\pm} + \Delta H_{14}^{\mathrm{ads}}(\mathrm{SiAl})$, and according to the evaluation detailed above, we obtained $\Delta H_{14}^{\mathrm{ads}}(\mathrm{SiAl}) = -23$ kcal mol^{-1}.

On combining Eqs. (2) and (3), the preexponential factor k_j^0 appears as

$$r_j = k_j C_j = k_j^0 \exp\left(\frac{-\Delta H^{\pm} - \Delta H_j^{\mathrm{ads}}}{kT}\right) C_j \tag{8}$$

with

$$k_j^0 = \frac{kT}{h} \exp\left(\frac{\Delta S^{\pm} + \Delta S_j^{\mathrm{ads}}}{k}\right) \sigma^*. \tag{9}$$

k_j^0/σ^* has units of (s^{-1}). From the experimental rate of 12×10^{-2} (mole of reactant)(g of catalyst)$^{-1}$ h^{-1} in Table 3, we know that k_{14} should be of the order of 0.8 (cm^3 of reaction volume) s^{-1} (g of catalyst)$^{-1}$ for a catalyst based on a FAU 1 zeolite, as the initial reactant concentration is 4.33×10^{-6} mol cm^{-3}. Using $\sigma^* = 25$, the measured acidity, as a normalization factor in arbitrary units, and with loading densities of about 1 g cm^{-3} for experimental catalysts (extrudates, diameter 1.4 mm), we obtain $k_{14}/\sigma^* \cong 3 \times 10^{-1}$ s^{-1}. With $kT/h \cong 1 \times 210^{13}$ s^{-1} at 573 K, and $\exp((-\Delta H_{14}^{\mathrm{ads}}(\mathrm{FAU}) - \Delta H^{\pm})/RT) = 10^{-3.63}$, this leads to $\exp((\Delta S^{\pm} + \Delta S_{14}^{\mathrm{ads}}(\mathrm{FAU}))/R) \cong 10^{-10}$ or $(\Delta S^{\pm} + \Delta S_{14}^{\mathrm{ads}}(\mathrm{FAU})) \cong -46$ cal mol^{-1} K^{-1}: we adopt this reasonable magnitude as a fitting parameter in order to input contact times consistent with experiments in the calculations which follow. Besides, it is possible to exploit the data

Table 4
Evaluation of adsorption entropies at 573 K from data in Table 1, assuming the validity of the Henry regime beyond a given value of V_m

	V_m (nm^3)	ΔS^{ads}(VFI) (cal mol^{-1} K^{-1})	ΔS^{ads}(BETA) (cal mol^{-1} K^{-1})	ΔS^{ads}(FAU) (cal mol^{-1} K^{-1})	ΔS^{ads}(VFI) (cal mol^{-1} K^{-1})
Phenanthrene	0.171	−49.9	−52.8	−57.6	−55.1
Methylcyclopentanodecalin	0.215	−60.3	−72.9	−59.5	−53.3
Perhydrophenanthrene	0.215	−69.6	−70.4	−56.8	−54.5
Dimethylcyclopentanomethylcyclohexane	0.227	−69.9	−59.8	−53.2	−53.8
Tetrahydrophenanthrene	0.227	−54.7	−66.0	−58.7	−51.2

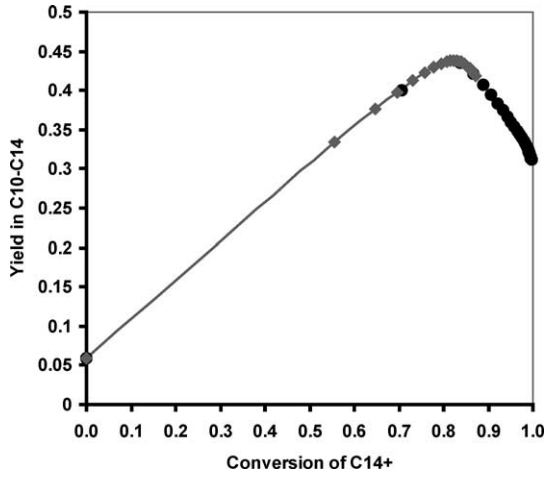

Fig. 6. Selectivity versus conversion plots for two model silica–aluminas differing only by the acid site density: $\sigma^* = 2$ and 20 (respectively, gray diamonds and black dots). The two graphs are superimposed ($\Delta\theta = 10^4$ s).

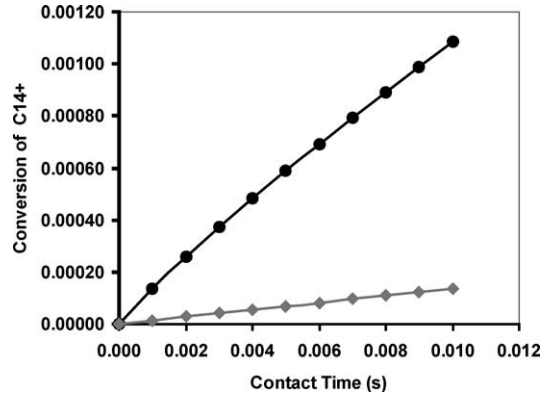

Fig. 7. Conversions versus contact time for the two model silica–aluminas presented in Fig. 6. $\sigma^* = 2$, gray diamonds, and $\sigma^* = 20$, black dots. The activity difference is reflected in the slopes here characterized at very low contact time ($\Delta\theta = 10^{-3}$ s).

in Table 1 in order to derive estimates of ΔS_j^{ads} at 573 K, since in the Henry regime, the equilibrium constant for adsorption is directly given by the ratio of concentrations in pores at equilibrium and in the gas phase, according to [3]: the Henry regime should be best obeyed for V_m approaching V_{mmax}, and applying this analysis we find indeed that ΔS_j^{ads} stabilizes between −50 and −60 cal mol^{-1} K^{-1} for $V_m > 0.2$ nm^3 for all zeolitic structures (Table 4). This implies that $\Delta S^{\pm}$ should be positive and of the order of 10 cal mol^{-1} K^{-1}, representing the modest gain in entropy upon going from the adsorbed state to the transition state for cracking. This gives us also some basis for the assumption that $(\Delta S^{\pm} + \Delta S_j^{ads})$ is independent of j. A more precise determination of entropic factors is, however, beyond the scope of the present paper.

In Fig. 6, we present the selectivity versus conversion plots for two model silica–aluminas differing only by the relative acid site density $\sigma^* = 2$ and $\sigma^* = 20$. The two graphs are superimposed. In Fig. 7, we have plotted conversions versus contact time for the two model solids, where we recover the order of magnitude of expected activity difference in the initial slopes. We show, therefore, that, within the assumptions of our model, selectivity at a given conversion is not determined by the acid site density, but rather by the adsorption versus molecular weight profile, as proposed in [1].

In what follows, we set the relative acid sites densities σ^* for zeolites according to the experimental results from [1] and [8] reproduced in Table 3. In absence of experimental information we have set equal values of σ^* for OFF and MFI, on one hand, and VFI and FAU, on the other hand. In Fig. 8,

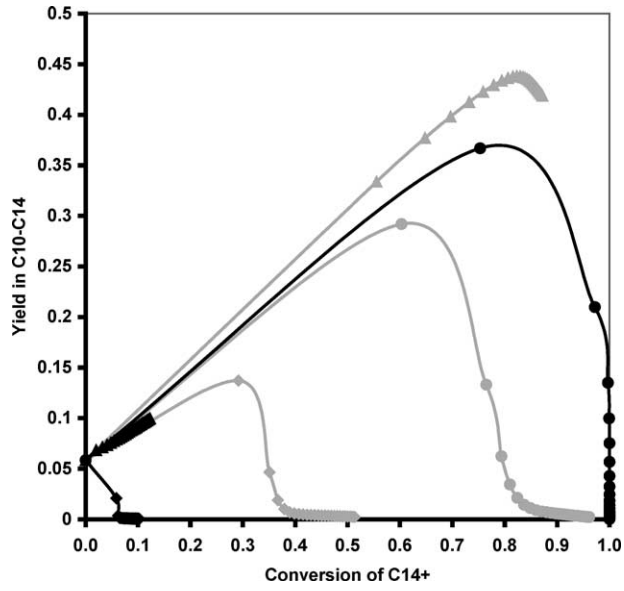

Fig. 8. Plots of selectivity versus conversion for a reference model silica–alumina with $\sigma^* = 2$ (gray triangles) and for zeolitic model catalysts with alumina binder (black triangles, MFI, $\sigma^* = 8.3$; black diamonds, OFF, $\sigma^* = 8.3$; gray diamonds, BETA, $\sigma^* = 14.5$; gray dots, FAU, $\sigma^* = 25$; black dots, VFI, $\sigma^* = 25$). We have set $\sigma^*/100$ for the binders. $\Delta\theta = 10^2$ s for zeolite-based model catalysts, and $\Delta\theta = 2 \times 10^4$ s for the silica–alumina model catalyst.

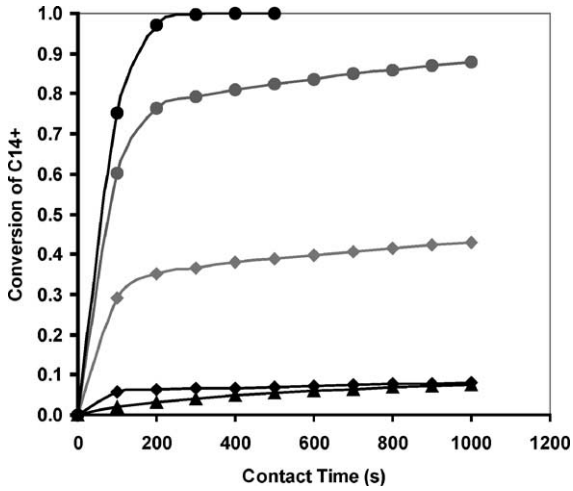

Fig. 9. Conversion versus contact time plots corresponding to Fig. 8 (black triangles, MFI; black diamonds, OFF; gray diamonds, BETA; gray dots, FAU; black dots, VFI. $\Delta\theta = 10^2$ s for all model catalysts.

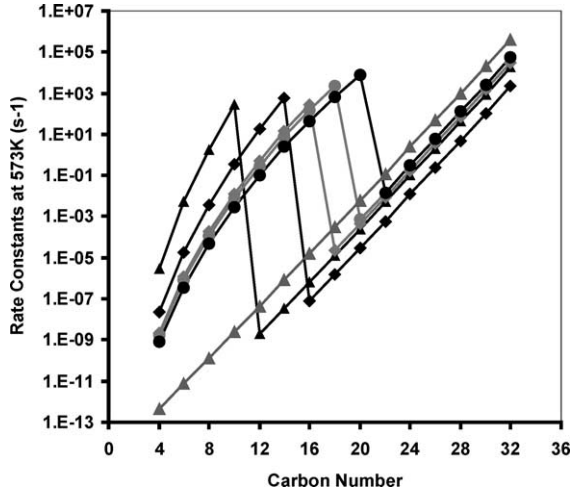

Fig. 10. Plots of $r(j)$ profiles which determine the results shown in Figs. 8 and 9. (Black triangles, MFI; black diamonds, OFF; gray diamonds, BETA; gray dots, FAU; black dots, VFI; gray triangles, model silica–alumina).

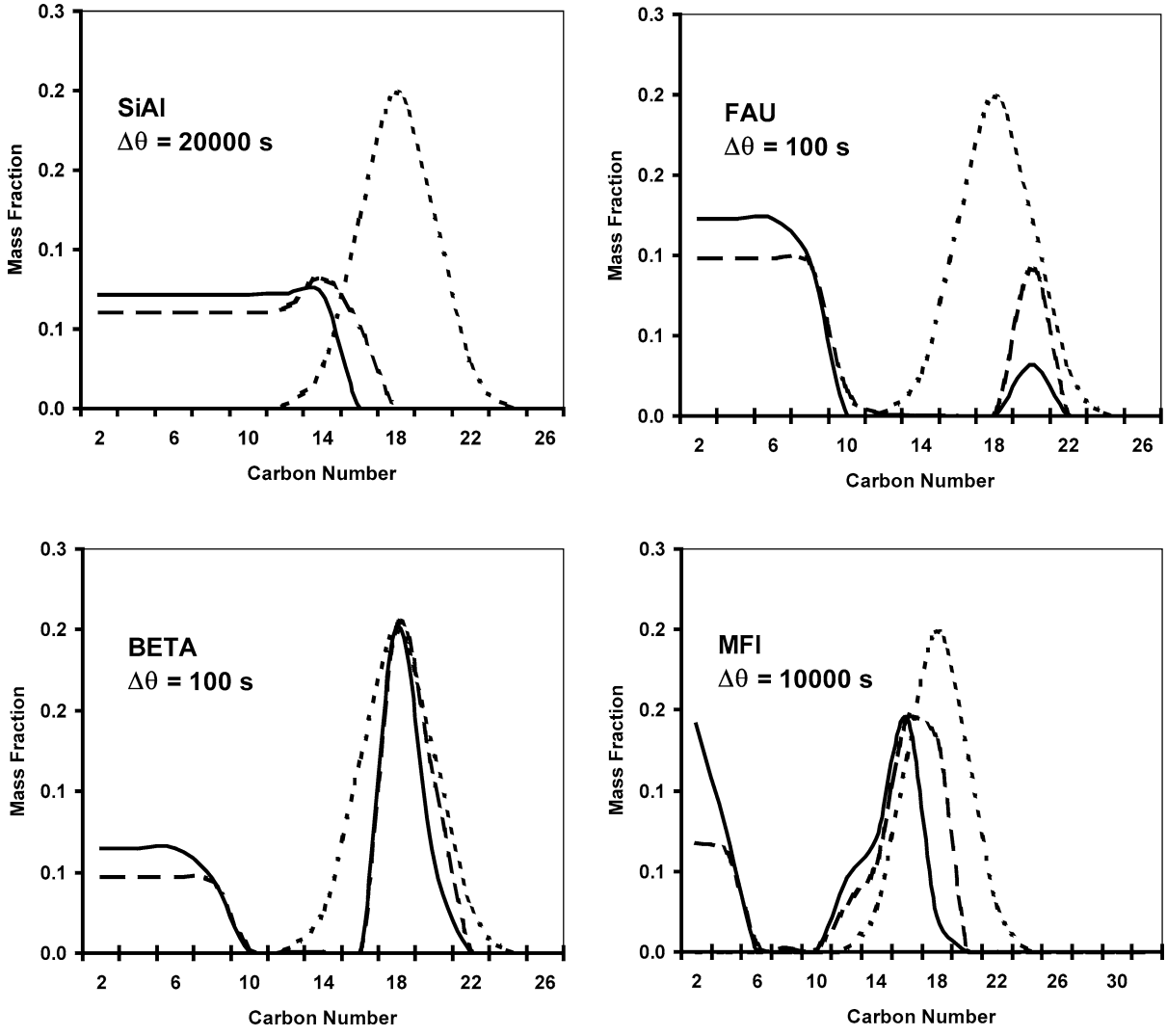

Fig. 11. Evolution of the distributions of hydrocarbons with increasing contact time ((- - -) 0, (– – –) 4, (—) 18 times $\Delta\theta$).

we compare selectivity versus conversion plots for a reference model silica–alumina ($\sigma^* = 2$), and for zeolitic model catalysts based on MFI, OFF, BETA, FAU, and VFI with alumina binder. We have set $\sigma^*/100$ for the binder. The residual acidity assigned to the alumina binder can be viewed as that brought about by the external surface of zeolite microcrystals. The corresponding conversion versus contact time plots are shown in Fig. 9.

These figures reproduce the essential features of our previously discussed experimental findings, as recalled in Table 3, namely selectivities at 60% conversion decreasing in the order

SiAl > FAU > BETA

while apparent activities are in the order

FAU > BETA > SiAl.

Fig. 10 shows the profiles $r(j)$ which determine these rankings in selectivity and activity: they are of course dominated by the confinement effects, through the exponential impact of the ΔH_j^{ads} profiles on the rates, according to Eqs. (1) and (2).

Fig. 11 shows the evolutions of the distributions of hydrocarbons with increasing contact times for SiAl, FAU, BETA, and MFI, respectively: these evolutions are determined by the profiles shown in Fig. 10 and provide the basis for the selectivity and activity patterns obtained. In the case of MFI, the gap in mass fraction at low carbon number is very apparent: it corresponds to a window of high activity determined by the confinement effect in this zeolite with the smallest pores. Interestingly, the initial selectivity observed of Fig. 8 for the hardly active MFI actually corresponds to that of the binder, and therefore parallels the selectivity obtained for the model amorphous silica–alumina.

It has been also shown in [1] that, in contrast with other solids (amorphous silica–aluminas and BETA-based catalysts with variable Si/Al ratios), an increase of selectivity was observed upon dealumination of the zeolite in FAU-based catalysts, while the activity decreased linearly with acidity. However, it is known that the dealumination technique (steaming) used in these experiments creates mesoporous voids inside the faujasite. This was indeed observed and reported for the samples compared in [1]. According to the present model, if the density of acid sites in the zeolite is decreased by a factor 42, as in the experiment (FAU 4), the selectivity, as defined here, hardly decreases, as shown in Fig. 12. If we allow moreover extra mesopores to be created by the dealumination process at the expense of the FAU framework, and keeping the low density of acid sites, we recover a selectivity and activity much higher than for the base case (see again Figs. 12 and 13). Indeed, the results of these simulations, which support the interpretation given in [1], stem from the fact that the confinement effect always dominates the activity profile, because of its exponential influence as compared to the linear influence of the acid site density. This has important practical consequences as it provides a guideline for the design of a hydrocracking catalyst with a prescribed selectivity with respect to the processing of a feedstock with a given molecular weight distribution. Our model should allow, for instance, the definition of an adequate pore size of the confining microporous solid to be combined with a proper density of Brønsted acid sites.

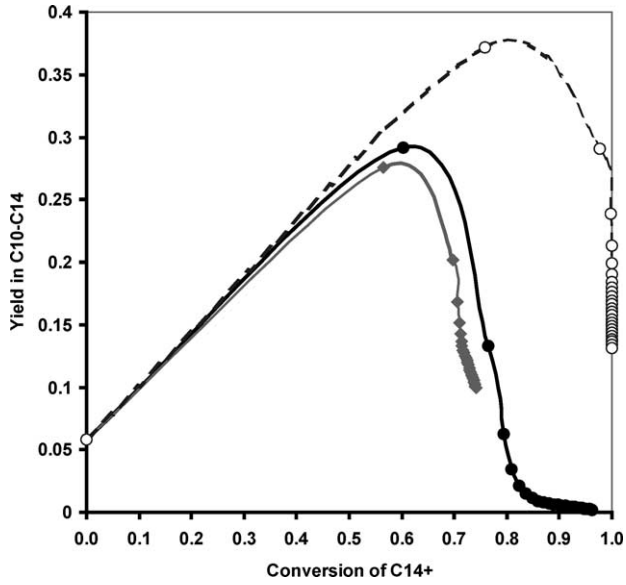

Fig. 12. Plots of selectivity versus conversion for FAU-based zeolitic model catalysts with alumina binder, showing the influence of dealumination. Black dots, FAU, reference case (same as in Fig. 8); gray diamonds, dealuminated FAU (FAU 2 in Table 3), with $\sigma^* = 0.6$ and $\sigma^*/100$ for the binder, without dealumination-induced extra mesopores; circles, dealuminated FAU with $\sigma^* = 0.6$ and $\sigma^*/100$ for the binder, with dealumination-induced extra mesopores, extra V_{mmax} arbitrarily corresponding to carbon number 22 ($\Delta\theta = 10^2$ s).

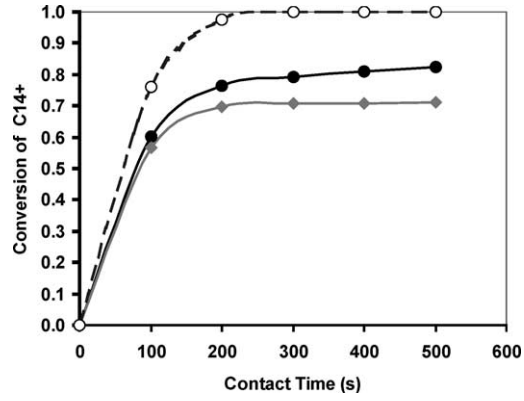

Fig. 13. Conversions versus contact time for the FAU-based zeolitic model catalysts presented in Fig. 12. The activity difference is reflected in the initial slopes. Black dots, FAU, base case (same as in Fig. 8); gray diamonds, dealuminated FAU with $\sigma^* = 0.6$ and $\sigma^*/100$ for the binder, without dealumination-induced extra mesopores; circles, dealuminated FAU with $\sigma^* = 0.6$ and $\sigma^*/100$ for the binder, with dealumination-induced extra mesopores, extra V_{mmax} arbitrarily corresponding to carbon number 22 ($\Delta\theta = 10^2$ s).

4. Conclusion

We have tried to capture in a simplified mathematical model the essentials of the confinement effects in hydrocracking. From this perspective we may conclude that for a given feedstock, characterized by an initial distribution function of hydrocarbon components according to molecular weight, it should be possible to define an optimum in terms of rate profile as a function of pore size, so as to achieve the best possible compromise between global conversion activity and the desired selectivity. The pore-size distribution (PSD) in the final catalyst is the most influential factor in achieving this.

References

[1] E. Benazzi, L. Leite, N. Marchal-George, H. Toulhoat, P. Raybaud, J. Catal. 217 (2002) 376.
[2] E.G. Derouane, J.M. André, A.A. Lucas, J. Catal. 110 (1988) 58.
[3] I. Derijcke, J.P. Vigneron, Ph. Lambin, A.A. Lucas, E.G. Derouane, J. Chem. Phys. 94 (1991) 4620.
[4] E.G. Derouane, J. Mol. Catal. A 134 (1998) 29.
[5] UFF and Sorption are distributed with Accelrys' software package Cerius^2 (Cerius^2 user guides and web site: http://www.accelrys.com).
[6] A.K. Rappe, C.J. Casewit, K.S. Colwell, W.A. Goddard III, W.M. Skiff, J. Am. Chem. Soc. 114 (1992) 10024.
[7] M.P. Allen, D.J. Tildesley, Computer Simulation of Liquids, Oxford Univ. Press, Oxford, 1989.
[8] L. Leite, PhD thesis, Université Pierre et Marie Curie (Paris VI) (2000).
[9] M. Schenk, S. Calero, T.L.M. Maesen, T.J.H. Vlugt, L.L. van Benthem, M.G. Verbeek, B. Schnell, B. Smit, J. Catal. 214 (2003) 88.